IJCRT.ORG ISSN : 2320-2882

INTERNATIONAL JOURNAL OF CREATIVE RESEARCH THOUGHTS (IJCRT)

An International Open Access, Peer-reviewed, Refereed Journal

Characterization Of The Solidification State Of Welded Cold-Formed Steels With Different Methods

M.Dadkhah[1], Th.Nitschke-Pagel[1], M.Zürn[2], J.Gibmeier[2]

[1]Institut für Füge- und Schweißtechnik (IFS), TU Braunschweig, Germany

[2]Institut für Angewandte Materialien (IAM-WK), KIT, Germany

Material strengthening that occurs during cold forming is an important means for increasing the stability of car body components. For this reason, different types of steel have been developed with increased strengthening potential in recent decades. A general problem occurs, if cold-formed components are joined by welding, since the welding locally resets the elaborately adjusted material condition. The present study investigates the interrelation of the strain hardening and the applied TIG (Tungsten-Inert-Gas) welding process, with a particular focus on a TRIP and a TWIP steel with high Mn contents. The investigations comprise hardness and microindentation tests as well as X-ray diffraction experiments of specimen that are pre-deformed to specific strains and subsequently TIG-welded with various linear energies. Instrumented microindentation tests are performed to determine force - indentation depth curves. The characteristic values derived from those curves are compared with results of a systematic peak profile analyses of measured X-ray interference lines. The results show that the measurement methods used enable detailed statements about the strengthening condition after cold forming and the local changes in the weld seam environment. Finally, the integral widths of X-ray diffraction lines can be correlated very well with distributions of local microhardness and can further be used to interpret the relationships between strain- and transformation-induced strengthening, deformation-induced retained austenite transformation and thermally induced softening. The results highlight the changes of the material states induced by welding and therefore emphasize the need to optimize welding practices and therefore improve the performance of high-strength steels in industrial applications.

1 Introduction

Modern deep-drawing steels have gained significant attention in materials science and engineering due to their exceptional properties, largely resulting from various strengthening mechanisms, particularly those induced by deformation. Cold deformation processes notably alter the material state, increasing dislocation density, yield strength (R_e), and material hardness. These changes are crucial for enhancing the mechanical performance of thin-walled structures. Additionally, the anisotropic behavior caused by cold working must be considered in the design and analysis of these structures, as it influences their response to external forces [1,2].

This study explores the TRIP (Transformation-Induced Plasticity) effect, which arises from the deformation-induced martensitic transformation of retained austenite, and the TWIP (Twinning-Induced Plasticity) effect, associated with deformation-induced twinning [3]. It also examines the influence of higher temperatures, such as those experienced during welding processes, on these mechanisms. The comprehensive analysis includes an investigation into the mechanisms driving these phenomena and their interplay and synergistic effects.

In pure carbon steels, the hardening achieved through cold deformation is based on the multiplication of dislocations as a result of plastic deformation. The newly formed dislocations create obstacles to sliding for subsequent dislocations and thus lead to a measurable increase in the yield strength. At the same time, the further plastic deformation capacity decreases. This mechanism will be more effective with a lower yield strength ratio and it requires a sufficiently large plastic deformation capacity in the initial state. Two structural mechanical processes that are dependent on the stacking fault energy are responsible for the hardening ability of austenitic steels with a high manganese content, the TRIP and the TWIP effect. On the one hand, this is the double deformation-induced martensitic transformation γ (fcc) $\rightarrow$ ε (hdp) $\rightarrow$ α ' (bcc) (**Tr**ansformation **I**nduced **P**lasticity). The continuous formation of deformation martensite causes an increase in the hindrance of dislocation movements in the austenite and thus increasing hardening. The uniform formation of martensite at a constant rate of deformation is associated with large plastic strains [4]. As shown in [5], hardening decreases with increasing strain rate because the heat generated during plastic deformation cannot be dissipated quickly enough and therefore the martensite transformation comes to a standstill more quickly due to an increase in the stacking fault energy.

However, the alloy concept with high Mn, Al and Si contents used in these steels has now largely been abandoned by manufacturers. Instead, TRIP steels currently have a ferritic-pearlitic appearance after hot rolling, with C contents having a mass fraction of around 0.2% and Al+Si contents of around 1.5%. Annealing in the two-phase region $\alpha+\gamma$ and subsequent not too rapid cooling to 600…700°C result in recrystallization, cementite dissolution, ferrite grain growth and the accumulation of carbon in the austenite. In the second step, rapid cooling takes place to a temperature at which isothermal bainite formation is to be achieved without precipitation of carbides and alloying elements. This leads to an enrichment of carbon in the remaining austenite and to austenite stabilization, so that after complete cooling, there is a retained austenite content of 5...15% depending on the alloy content in a ferritic-bainitic matrix [6,7].

The second deformation mechanism is mechanical twinning (Twinning Induced Plasticity, TWIP effect). The adaptation deformations necessary for plastic deformation are carried out by folding over adjacent grid areas at a shear angle that depends on the grid structure. In the austenitic lattice, the slip planes of type {111} form the mirror or twin planes. The parts of the crystallite reflected on the mirror or slip plane form a coherent transition with a changed crystal orientation (twin plane), which ultimately acts like a grain boundary and hinders dislocation movement. This results in a macroscopically increased strength [8] and the effect is also known as the dynamic Hall-Petch effect [9–11]. The continued shifting of the deformations leads to very high elongations at break and a low yield strength ratio in these steels. With regard to the expected fatigue resistance, it is important to note that according to [12], internal compressive residual stresses are expected in all directions in the crystallites affected by twinning.

Twinning is associated with a change in the stacking sequence and preferentially begins in the stacking fault environment. The required shear stress, therefore, depends primarily on the stacking fault energy. At low stacking fault energies, deformation-induced martensitic transformation can occur, while with increasing stacking fault energy, twinning tends to predominate. Both slipping and twinning are mechanisms that accommodate plastic deformation, with deformation-induced transformation being a special case within this context. The stacking fault energy is largely determined by the chemical composition, with the Al and Si contents being particularly important in this group of materials [13].

While cold forming processes enhance the mechanical properties of deep drawing steels, welding presents several challenges. The localized heating during welding initiates complex material transformations that require thorough investigation. Temperature gradients from welding can cause phase transitions, recrystallization, and formation of new phases, significantly affecting material characteristics. Additionally, annealing effects from welding can alter hardness, strength, and microstructure of the material, which necessitates a detailed study of their impact on welded components [14].

Addressing the challenges posed by welding and its effects on material state is central to this research. The objective is to advance engineering practices by elucidating the intricate relationship between welding and material properties, ultimately enabling the design and production of robust, high-performance, thin-walled components with extended service life.

Fig. 1 schematically illustrates the methods employed in this study to determine the mechanical characteristics of the investigated steels, providing a visual overview of the experimental approach. The aim of the investigation was to analyze the potential for integrating methodologies that address both macroscopic and microscopic scales in order to explore the behavior of steel under deformation and welding heat cycles. The combination of hardness determination, instrumented microindentation, and X-ray interference line profile analysis was evaluated to allow for a more comprehensive characterization of the mechanical properties of the investigated materials. These findings are expected to enhance the understanding of the respective material response to various loads.

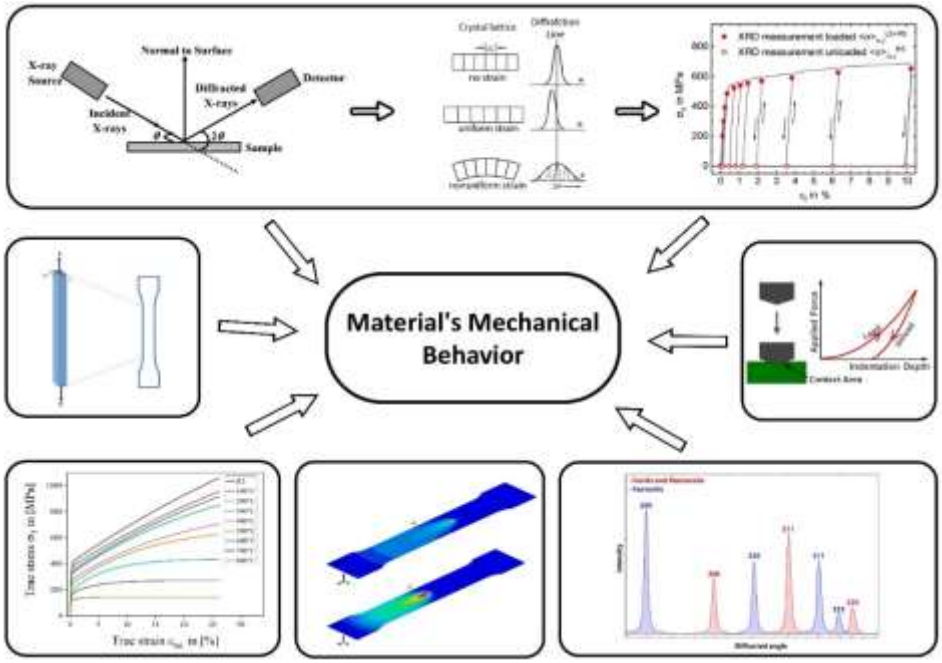

Fig. 1 Methods Employed in This Study for Determining Mechanical Characteristics of Investigated Materials

2 Experimental Procedures, Materials, and Objectives

To ensure a comprehensive analysis, three distinct steel grades were selected, each offering unique properties and challenges. This selection includes an in-depth examination of TRIP and TWIP steels, focusing on their specific characteristics and comparing them with traditional structural steels like S355MC which is used as a reference point to better understand how these materials respond to welding and deformation-induced microstructural changes.

The investigated materials encompass a variety of steel grades, each with distinct compositions and properties. HCT690T (TRIP700), a low alloy steel, is noted for its higher carbon content and approximately 12% retained austenite in its initial microstructure. This feature provides significant strengthening potential due to the transformation propensity of retained austenite into martensite under specific factors such as temperature, pressure or stress levels necessary for the transformation. X40MnCrAlV-19 2.5 2 (TWIP), a highly alloyed austenitic steel, contains a substantial carbon content and various alloying elements, adding complexity and making it central to the investigation [15]. Lastly, S355MC, a micoalloyed steel with minimal strengthening potential, is characterized by a low carbon content and provides a clear baseline, independently of alloying influences.

The selection of these steel grades offers a comprehensive perspective on the various material behaviors under welding heat cycles and deformation-induced changes. Table 1 summarizes the chemical compositions of the test materials for reference and comparison. Additionally, Fig. 2 illustrates the stress-strain curves for the investigated materials. The tests were carried out in both the rolling direction (RD) and the transverse direction (TD) to exclude an influence of a deformation texture possibly induced by the deep

rolling procedure of the initial plates. The illustrated stress-strain curves represent the average values of five samples each.

Table 1 Chemical Composition of the Test Materials

S355MC

Mass fraction (%)	C	Mn	Si	P	S	Cu	Al	Nb	V	Ti
OBLF-Spec.	0.022	0.161	0.034	0.010	0.005	0.056	0.046	0.028	0.007	0.003

HCT690T

Mass fraction (%)	C	Mn	Si	P	S	Al	V	Cu	B	Ti+Nb	Cr+Mo
OBLF-Spec.	0.176	1.793	0.366	0.011	0.006	1.279	0.008	0.026	0.0001	0.022	0.02

X40MnCrAlV 19 2.5 2

Mass fraction (%)	C	Mn	Si	P	S	Al	Cr	Ti	V	Cu	Ni
OES-Spec.	0.377	18.62	0.246	0.019	0.0040	1.09	1.68	0.02	0.115	0.038	0.066

The experimental program included investigations of the initially cold formed and then welded condition. To investigate the influence of the welding induced thermal load on the strengthening condition and its changes, a Tungsten-Inert-Gas-(TIG) welding process was performed. Bead-on-plate welds (dummy seams) were placed on the samples to avoid the influence of additional filler material. This procedure is representative of practical applications for thin plates, which are typically welded as overlap joints without filler material. To apply different temperature loads, the heat input was varied by adjusting the welding current and voltage, while the welding speed was kept constant. A comparative analysis of the different thermal loads was performed using both the calculated and measured cooling rates during welding. For the characterization of the temperature loads, the so called $t_{8/5}$-time, which represents the cooling curve between 800 and 500°C, was used [16]. The applied welding parameters and the resulting heat input and $t_{8/5}$-times are summarized in Table 2.

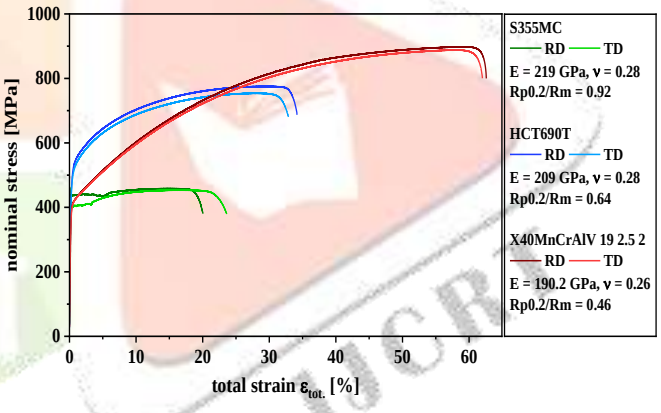

Fig. 2 Stress–Strain Curves for the Investigated Materials in Rolling Direction (RD) and Transverse Direction (TD)

Table 2 Welding Parameters

Material	plate thickness [mm]	welding speed [cm/min]	voltage [V]	welding current [A]	heat input [kJ/cm]	$t_{8/5}$ [s]
S355MC	2	30	9.1	50	0.91	0.83
			9.4	75	1.41	1.43
			10.3	100	2.06	2.45
			11.52	125	2.88	3.67
			12.03	150	3.61	4.26
HCT690T	1.75	30	9.1	50	0.91	1.84
			9.4	75	1.41	2.49
			10.3	100	2.06	3.06
			11.16	112	2.50	3.66
			11.52	125	2.91	4.32
X40MnCrAlV 19 2.5 2	2	30	9.1	50	0.91	1.59
			9.4	75	1.41	2.41
			10.3	100	2.06	3.87
			11.52	125	2.88	4.01
			12.03	150	3.61	4.23

shielding gas: 100% Ar / flow rate = 12 l/min

To understand the behavior of TRIP and TWIP steels during deformation and welding heat cycles, a multifaceted approach is adopted. This strategy aims to assess the mechanical responses of these steels through various tests, including hardness testing, instrumented indentation testing, and X-ray interference line profile analysis. It is essential to evaluate the changes in mechanical properties under different conditions, such as in not welded but deformed, and welding under deformation condition.

Utilizing hardness determination and instrumented microindentation testing provides a dual-layered analytical framework, capturing both broad mechanical characteristics and localized material property variations. Hardness serves as a general indicator of material properties, while results of instrumented microindentation testing discloses supplementary and detailed information on localized microstructural changes induced by welding [17].

X-ray interference line profile analysis is employed to offer a sophisticated description of the post-welding state and evaluate the suitability of steels in welded structures. This method examines X-ray diffraction intensity profiles to yield valuable data on crystalline structures, such as the presence of defects, strain, or texture. For instance, peak broadening in X-ray diffraction lines often results from reduced domain size and increased micro-strain. While asymmetric peak shapes are typically associated with strain gradients, stacking faults, or coarse grain effects. Crystallite orientation or texture primarily affects the relative intensities of the diffraction peaks. Furthermore, comprehensive understanding of alterations in peak positions (2θ), peak widths (which contains information about domain size, micro-strain distribution, and dislocation density) and peak intensities requires more complex models and equations. These extend beyond the fundamental Bragg's equation, which primarily determines the conditions for diffraction of X-rays at a crystal lattice. In particular, for the calculation of dislocation densities, the single line profile analysis method has been utilized [18]. This method involves analyzing the Fourier coefficients of line profiles and distribution moments, which allows for the extraction of dislocation density (ρ) along with other important microstructural characteristics [19,20]. Therefore, a standard ψ-diffractometer with a 2mm pinhole collimator and a position sensitive line detector (PSD) was used to determine the {211}-diffraction lines of the ferrite/martensite phase using CrKα–radiation and the {311}-diffraction lines of the austenite (TWIP-

steel) with MnKα–radiation. For the deconvolution of the apparatus specific influence and the physical diffraction lines, a reference standard sample of a low carbon steel C10 in the weakly annealed condition was used. The determination of the retained austenite content (TRIP-steel) was also performed using XRD by means of the 6-line analysis [21]. Here the {200}-, {220}- and {311}- (austenite) and the {200}-, {211}- and the {321}-diffraction lines (ferrite/martensite) where determined using MoKα–radiation. Due to the small carbon content of the TRIP-steel and the almost cubic structure of the martensite, the diffraction lines of ferrite and martensite were evaluated consistently.

Hardness measurements were performed using a standard Vickers hardness [22] tester and a force of 5 N (HV0.5), the instrumented microindentation tests were carried out using a Fischerscope microindentation testing system type HM2000 from Helmut Fischer GmbH (Sindelfinden, Germany). The force - indentation depth curves were determined within a force range of 2000 mN, with an indentation and release duration of 40 seconds. To achieve a more uniform distribution of values, the distance between measuring points was consistently set at 300 µm, with each point positioned 250 µm away from the welded edge of all specimens. For the evaluation of the different strengthening conditions, the integral breadth IB of the physical X-ray diffraction line profile and the derived domain size D, dislocation density ρ and micro-strain ε were used. Additionally, the results of the hardness measurements and the instrumented indentation experiments were considered.

To illustrate the outcomes derived from instrumented microindentation [23], the total indentation work amounts (in µJ) were calculated. The total indentation work (W_t) quantifies the energy expended during the indentation process and is calculated as follows:

$$W_t = W_p + W_u$$

Where W_p represents the plastic work part associated with irreversible deformation, and W_u denotes the elastic work part, which is recoverable upon unloading [24].

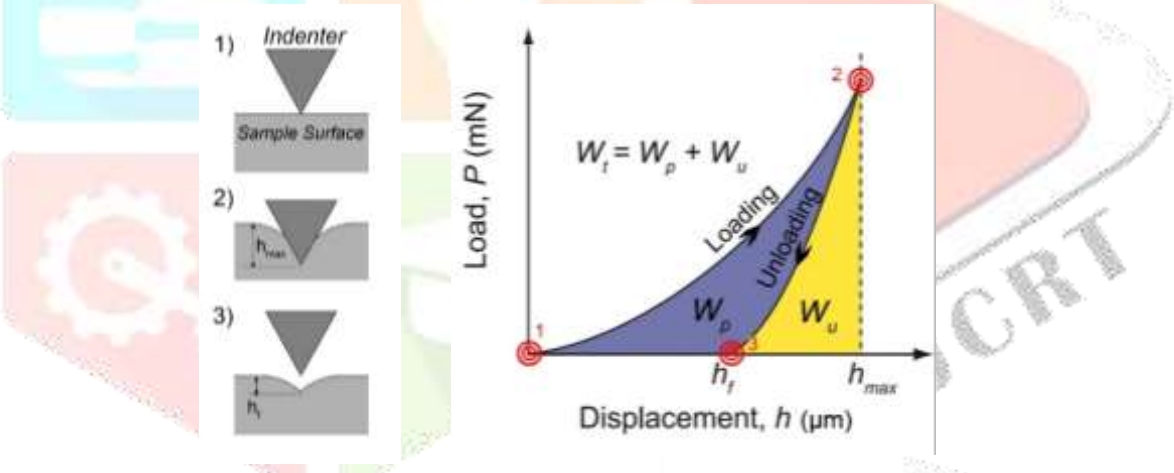

Fig. 3 Schematic Representation of (Left) the Indentation Stages, Including the Maximum Indentation Depth (h_{max}) And the Final Depth (h_f), And (Right) the Corresponding Load-Displacement Curve

3 Results and Discussion

Assessing the Initial and Deformed Conditions

Fig. 4 illustrates the relationship between the mechanical hardness and X-ray diffraction line breath of various steels over the total deformation. The hardness is observed to increase almost linearly with the extent of deformation, correlated with the increase in dislocation density induced by plastic deformation, in conjunction with the martensitic transformation in HCT690T. Notably, this transformation begins significantly at a total strain of approximately 2%, as shown later in Fig. 8.

The reference steel S355MC shows only a low dependency between hardness and plastic deformation as expected referring to the stress-strain behavior shown in Fig. 2 which indicates an almost ideal elastic-plastic behavior.

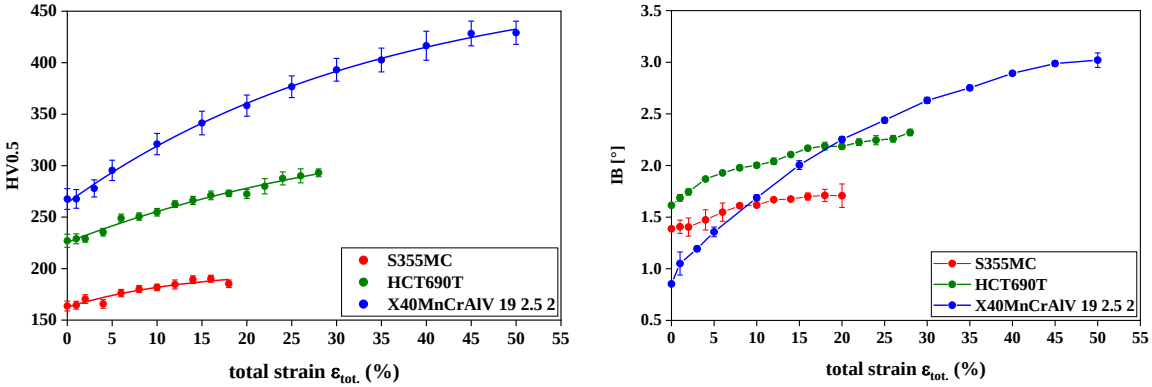

Fig. 4 (Left) Small load Vickers Hardness HV vs. Total Strain, (Right) Diffraction Line Breadth IB vs. Total Strain

The determined integral breadths of the measured XRD diffraction lines show not only a similar characteristic behavior. It can be seen that integral breadth and hardness correspond almost linearly, as shown in Fig. 5. As the curves reveal the pure comparison of the integral breadth and the measured hardness dependency cannot be used quantitatively, but for a qualitative evaluation of the hardening condition the use of the non-destructive determination of the integral breadth is suitable.

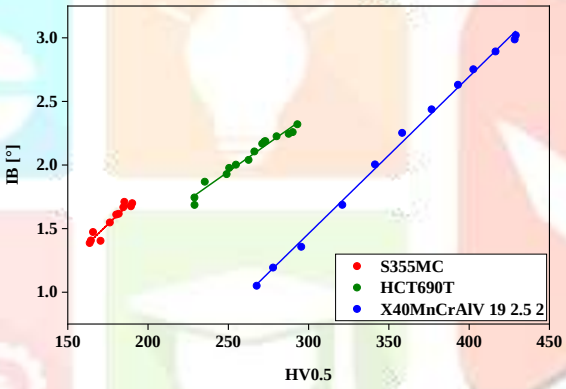

Fig. 5 Correlation of Hardness and XRD Diffraction Line Breadth IB vs. HV

The next investigative step was to analyze the change or the stability of the deformation dependent hardening condition of the different steels under a thermal load. Here, temperature loads which may occur

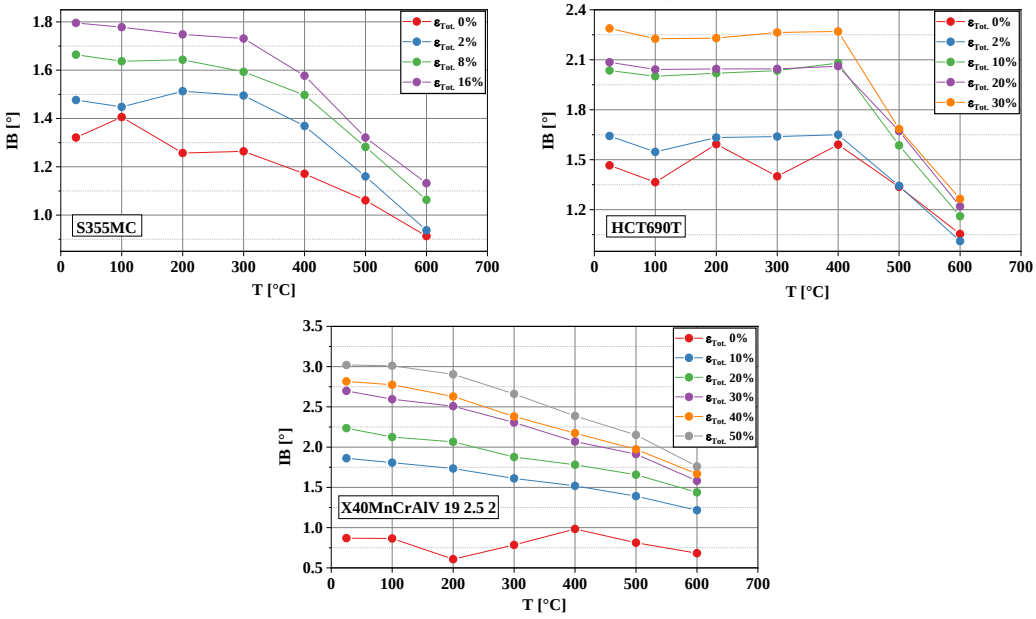

Fig. 6 Effect of Temperature and Deformation Degree on Integral Breath of the Diffracted Peaks

in the surrounding of the weld seam in the adjacent base material were applied on the investigated base material samples and the strengthening condition was characterized qualitatively by means of the integral breaths IB from the X-ray diffraction lines. As Fig. 6 reveals, the integral breadths determined for the ferritic steels remain nearly stable up to about 300°C for S355MC and 400°C for HCT690T. At higher temperatures, the decreasing integral breadths indicate softening for both steels due to material recrystallization, along with a decline in martensite content in HCT690T. The austenitic steel exhibits a slight softening starting from a temperature of about 100°C, with an increase in the slope around 200°C.

Welding Assessment for Initial and Deformed Conditions

The micrographs of the investigated welds shown in Fig. 7 give an overview of the microstructural changes in the weld zone after welding with different heat inputs, as listed in Table 2. As the heat input increases, the depth of the molten zone also increases, and the adjacent heat-affected zone, where temperatures are below the melting point but above A_{c1}, becomes wider. Despite the uniform heat input at each level the size of the molten and the heat affected zones is not strictly uniform. This is due to the differences of the resulting $t_{8/5}$-times caused by the different thermal conductivity of these steels and finally also due to the slight lower

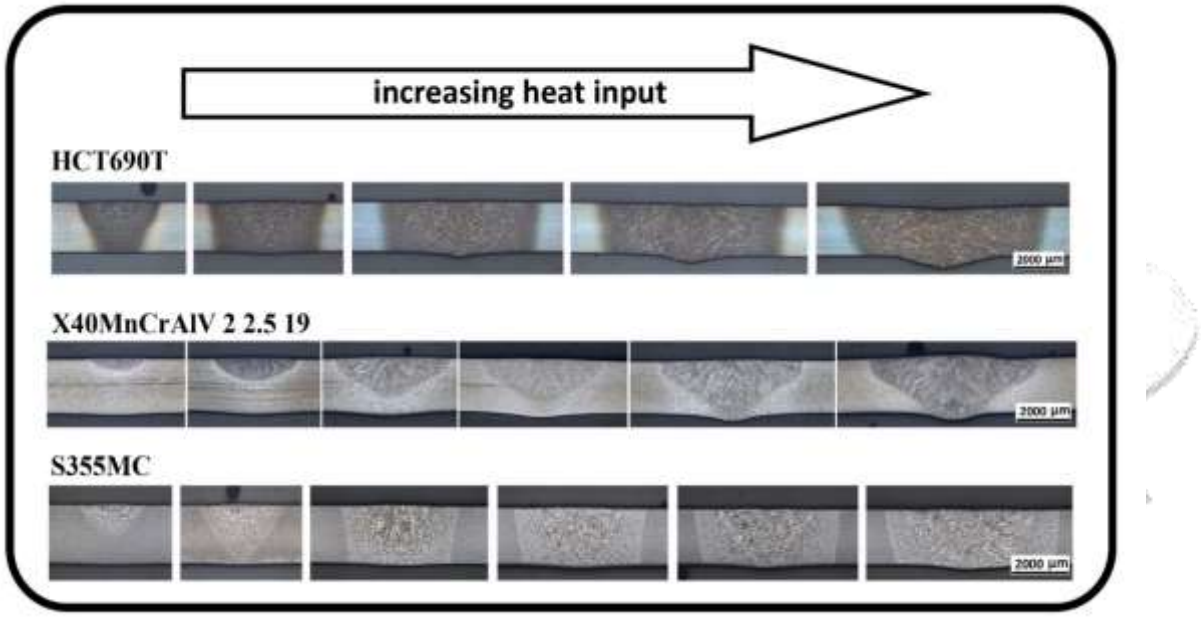

Fig. 7 Micrographs of Investigated Welds Under Varying Heat Input

plate thickness of the TRIP-steel materials.

Fig. 8 presents the distributions of the content of retained austenite in HCT690T-samples, both as measured and normalized values, which are referenced to the non-deformed base material. The initial constant is

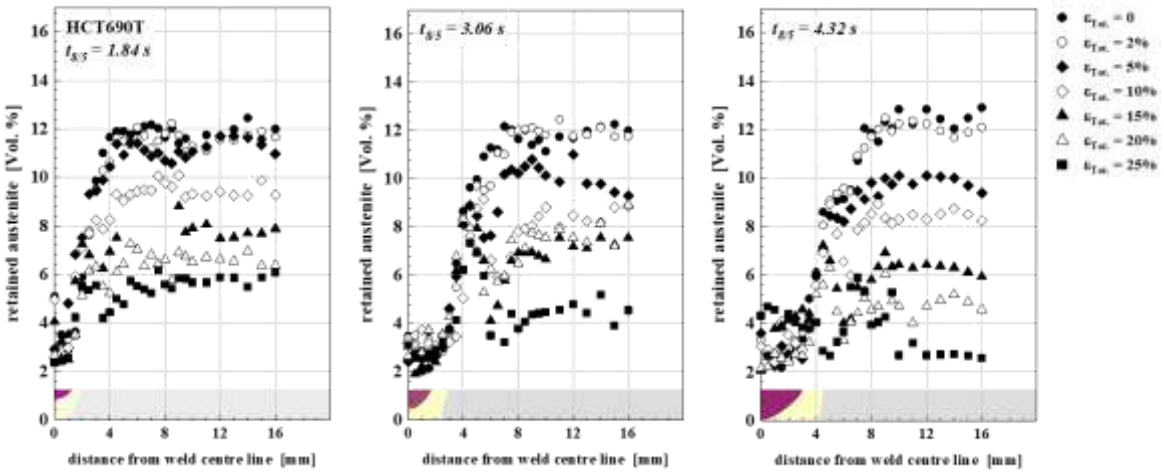

Fig. 8 Local Content of Retained Austenite in HCT690T After Welding of Differently Deformed Samples with Varying Heat Inputs

approximately 12% which is in the range expected for this type of steel. The values determined in the base material indicate that the deformation-induced austenite transformation begins at total strains of about 2%, with the remaining content continuously decreasing as the plastic deformation increases. In the weld seam no significant content of retained austenite above the detection limit can be found. Next to the heat affected zone the content arises quickly in all samples. The base metal level is reached 4 to 8 mm away from the weld center, depending on the heat input. In the base metal the distributions show no significant dependency of the heat input which is comprehensive because the maximum temperatures in this region did not exceed 300°C during welding. Consideration must be given to the potential errors and uncertainties inherent in the 6-line methodology used in this study for calculating the retained austenite content [21]. Factors such as peak overlap, degree of crystallographic texture, and variations in measurement conditions can influence the precision of this method, thereby introducing a degree of uncertainty to these results. Thus, the interpretation of these findings should carefully consider this potential deviation.

Fig. 9 shows the normalized hardness distributions of the welded specimens HCT690T and X40MnCrAlV 19 2.5 2, which are referenced to the non-deformed base material hardness. This normalization scale facilitates the comparison of strengthening conditions while minimizing the effects of scattering in hardness values. The same approach was applied to normalize the indentation work determined on base of instrumented indentation testing, see Fig. 10.

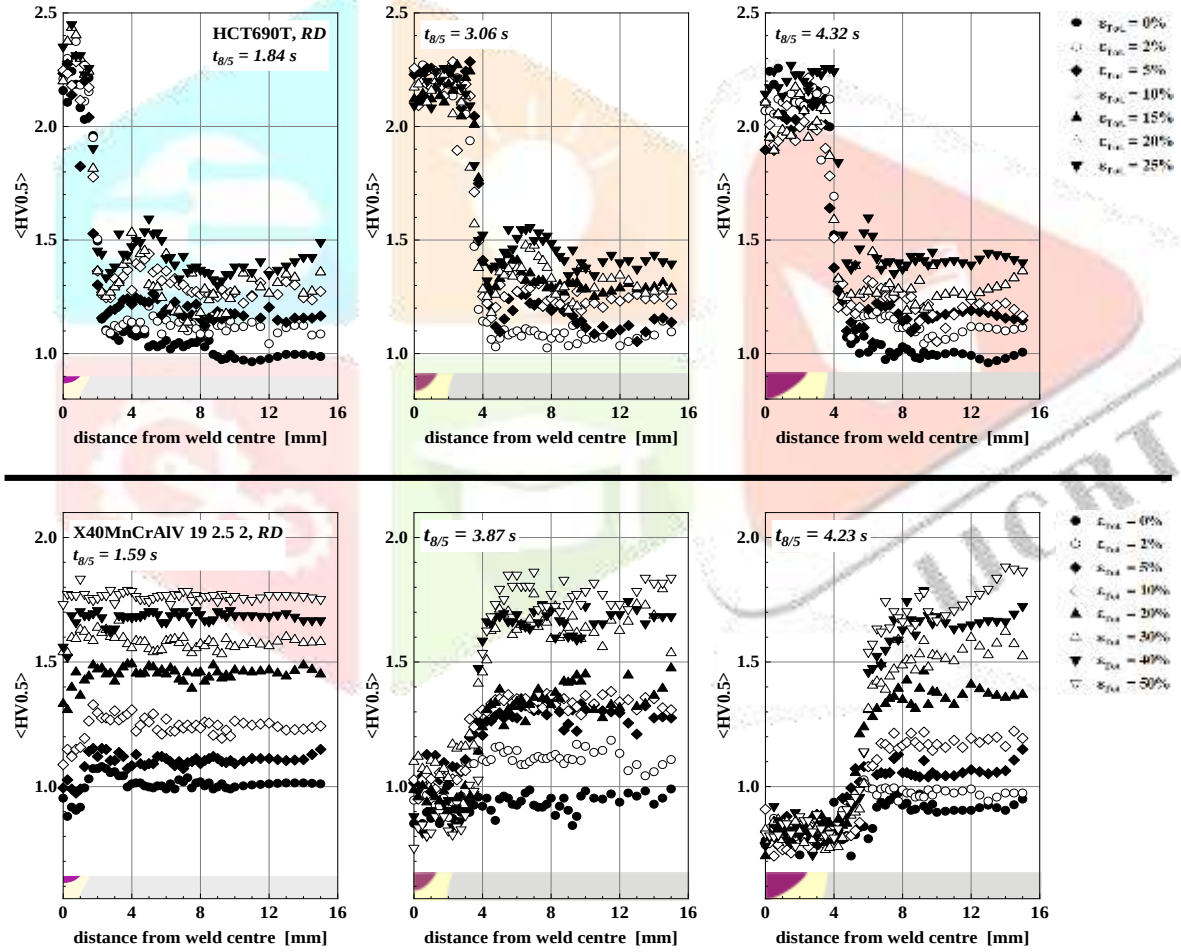

Fig. 9 Hardness Distribution of (Top) HCT690T and (Bottom) X40MnCrAlV 19 2.5 2 Under Varying Heat Input (Increased from Left to Right) in Different Deformation Grades (normalized to the non-deformed base material)

The results of the S355MC are not considered here, because due to the low carbon content and the almost ideal elastic stress-strain behavior in this steel no remarkable changes of the materials hardness were observed, neither due to the different heat input nor due to the deformation grade.

In examining the distribution of hardness and maximum indentation work across the welding area for HCT690T, as depicted in Fig. 9 and Fig. 10, it is observed that both the hardness and the results of instrumented microindentation testing consistently show little dependence on the applied cooling times. This consistency underscores the robustness of the mechanical properties of the materials under varying thermal conditions in accordance with determined retained austenite distributions. The data from both methods indicate significant hardening in the transformed regions, which can be attributed to the rapid austenite-to-martensite transformation that occurs during cooling [14]. The observed stability in mechanical properties, regardless of cooling duration, highlights the reliability of HCT690T for applications that experience different thermal cycles.

Further analyses of steel X40MnCrAl 19 2.5 2, as illustrated in Fig. 9 and Fig. 10, reveal a marked reduction in hardness within the weld seam area following pre-existing deformation.

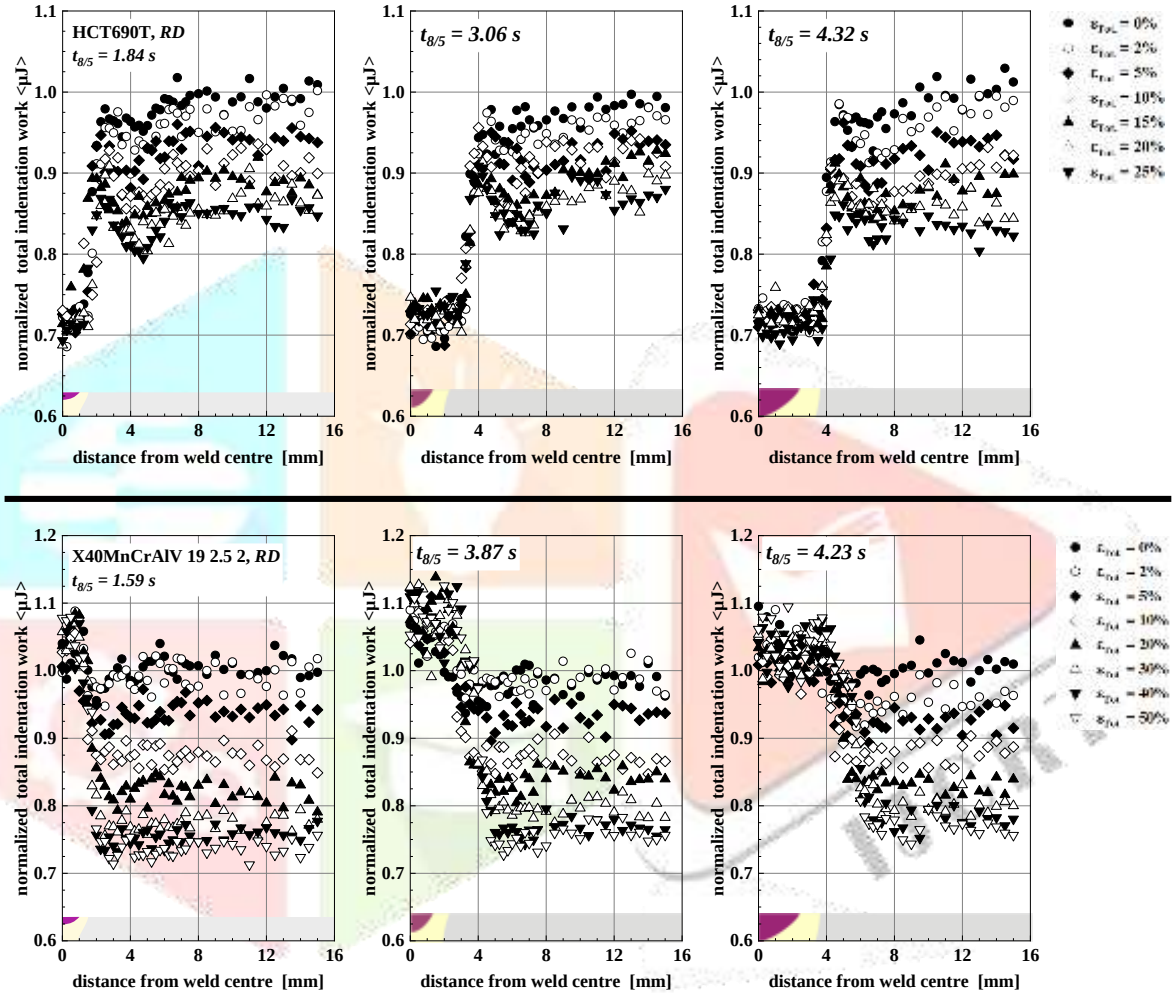

Fig. 10 Normalized Total Indentation Work Distribution of (Top) HCT690T and (Bottom) X40MnCrAlV 19 2.5 2 Under Varying Heat Input (Increased from Left to Right) for Different Deformation Grades (normalized to the non-deformed base material)

This comparative study illustrates the distinct responses of HCT690T and X40MnCrAlV 19 2.5 2 steels under similar thermal and deformation conditions. Both materials exhibit increased strengthening with higher deformation levels. However, thermal conditions have differing impacts: within the welding and heat-affected zone (HAZ), X40MnCrAlV 19 2.5 2 tends to soften, possibly due to grain coarsening [24], whereas HCT690T demonstrates increased hardening, possibly due to phase changes or grain refinement.

Diffraction Line Profile Analysis

The results, shown in Fig. 11, indicate that the IB of the X-ray interference lines for HCT690 is largely unaffected by the applied cooling times. In other words, increasing welding energy leads to only a minor increase in IB across different deformation degrees, suggesting the stability of the material under thermal variation. The noticeable broadening of X-ray interference lines might initially suggest hardening due to the austenite-to-martensite transformation in HAZ. However, this apparent broadening could also result from the measurement spot size being large enough to include martensitic structures in the weld seam. This inclusion may influence the X-ray interference line measurements rather than solely reflecting transformations in the heat affected zone. Therefore, the observed broadening might be more accurately attributed to a 'smearing effect' rather than substantive phase transformations in regions without such

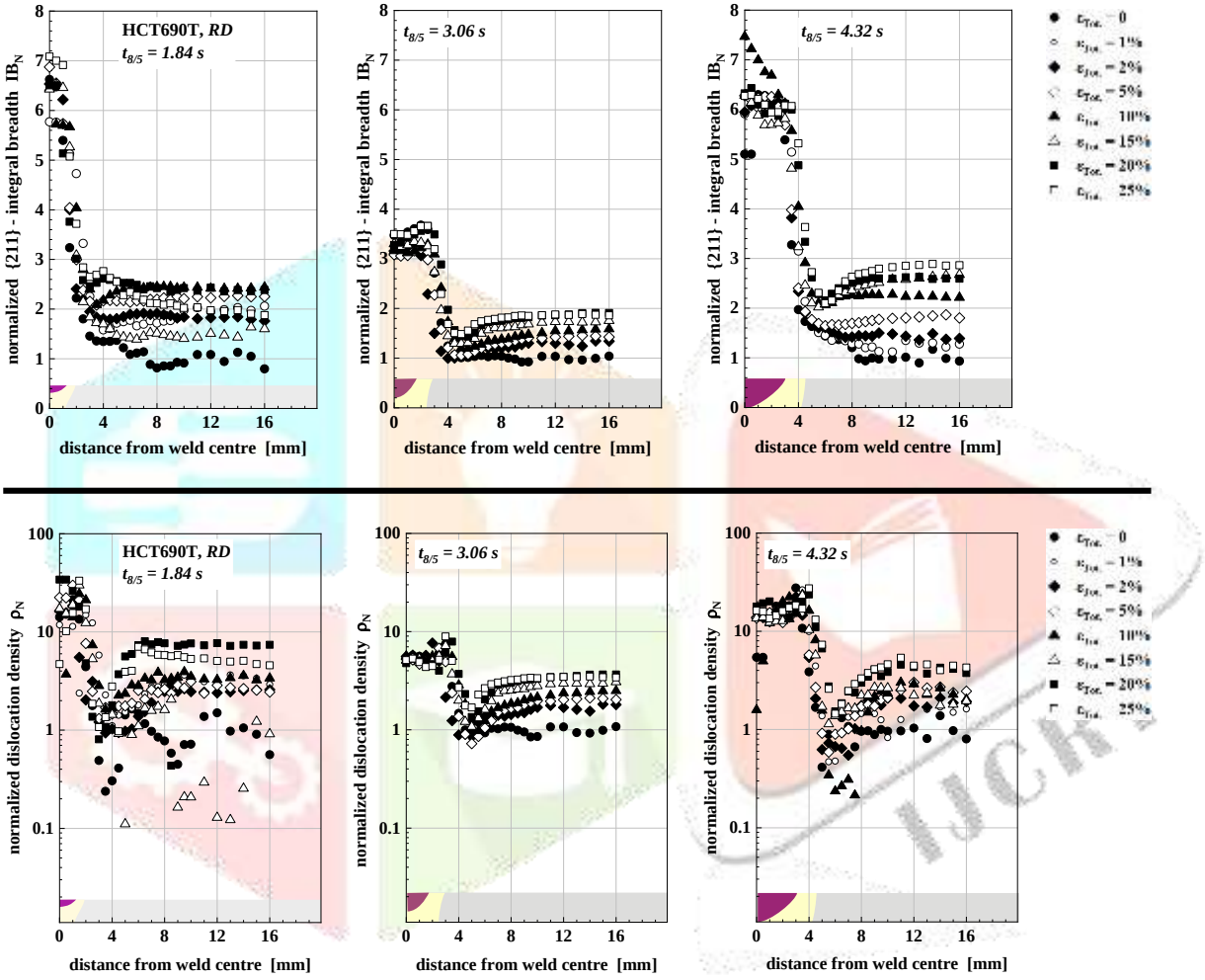

Fig. 11 Integral Breadth (Top) and Dislocation Density for the Martensite/Ferrite Phase (Bottom) of HCT690T Under Varying Heat Input (Increased from Left to Right) in Different Deformation Grades (normalized to the non-deformed base material)

changes.

Additionally, the dislocation density appears to be independent of welding energy, although there is noticeable increase in dislocation density in the welding area, which may be primarily due to martensitic transformation.

The distributions of the integral breadth IB determined in the austenitic X40MnCrAlV 19 2.5 2- steel indicate a strength behavior which stronger depends on the combination of different heat loads and the pre-deformation condition. While in the weld seam and in the nearby heat affected zone the course of IB vs. distance to the weld center shows a uniform softened level of course with different peak widths, i.e., the IB-values in the base material continuously increase with increasing heat input, as shown in Fig. 12.

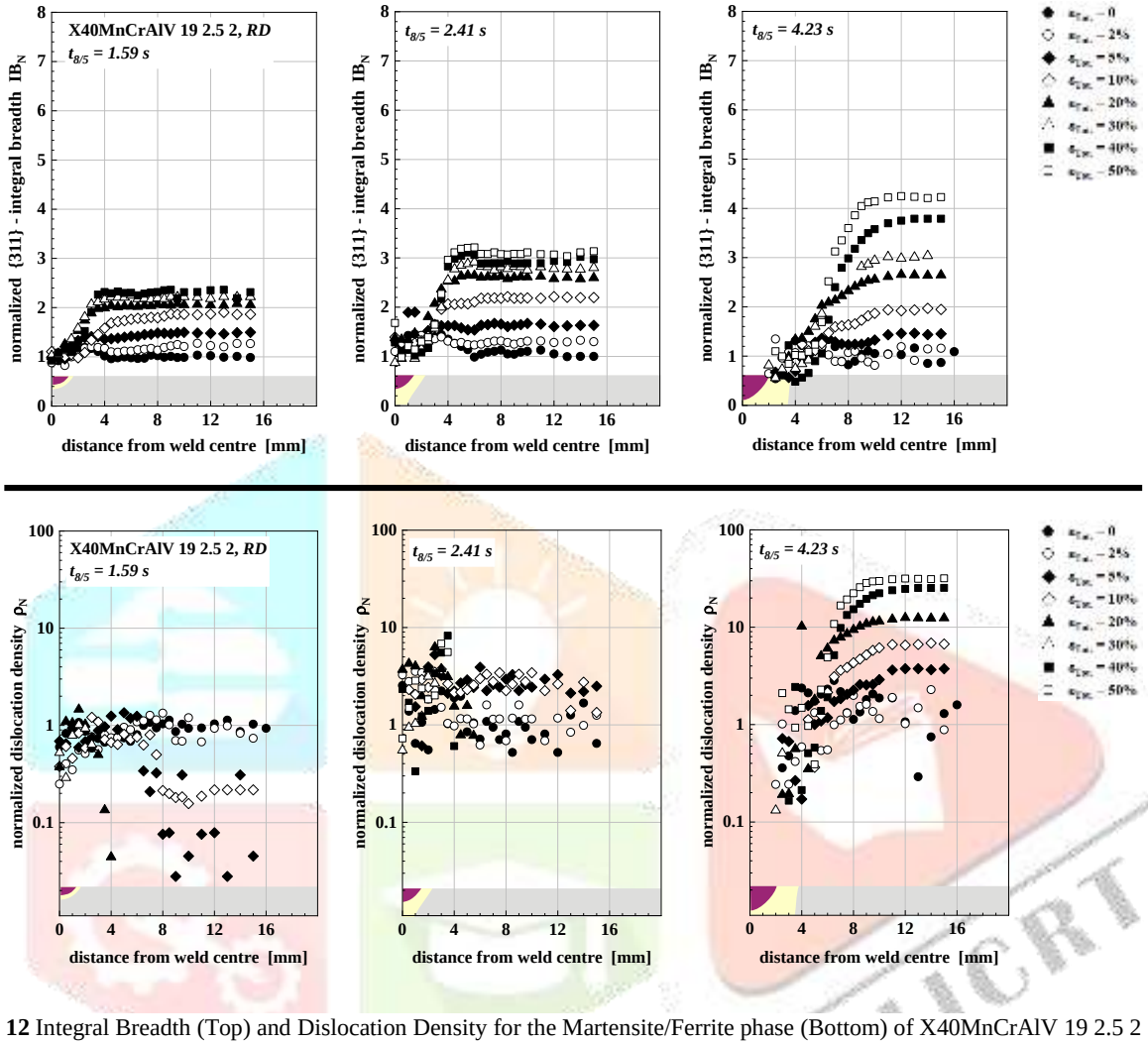

Fig. 12 Integral Breadth (Top) and Dislocation Density for the Martensite/Ferrite phase (Bottom) of X40MnCrAlV 19 2.5 2 Under Varying Heat Input (Increased from Left to Right) in Different Deformation Grades (normalized to the non-deformed base material)

This indicates that the constraints of the weld are important not only for the development of residual stresses. Evidently, the shrinkage of the weld zone in the cooling phase leads to localized plastic deformations in specific regions during cooling, resulting in a distinct increase of the resulting IB-values. Various microstructural processes, such as increasing grain size, may contribute to the observed softening effects in the transforming areas. The additionally considered distributions of the calculated dislocation densities principally agree with this observed behavior, although they exhibit stronger scattering.

Finally, the normalized distributions of the determined integral breadths and the calculated dislocation densities of the reference material S355MC are given in Fig. 13. The distributions appear nearly uniform, lacking any local minima or maxima. This is due to the low carbon content of the material, which leads to an austenite-ferrite transformation in the weld seam at relatively high temperatures. As a result, the microstructure does not contain any martensite or bainite resulting in almost no change in the calculated dislocation density. [25]. In the base material, a slight strain hardening effect is observed, depending on the degree of deformation, indicated by a small increase in dislocation density. The constraint appears to have a minor impact on the strength of the base material; however, the higher heat input affects the recovery of the cold-formed condition, resulting in a slight reduction in the integral breadth values. The calculated

dislocation densities exhibit similar behavior with a more nuanced resolution; however, the greater scatter of these values must be considered.

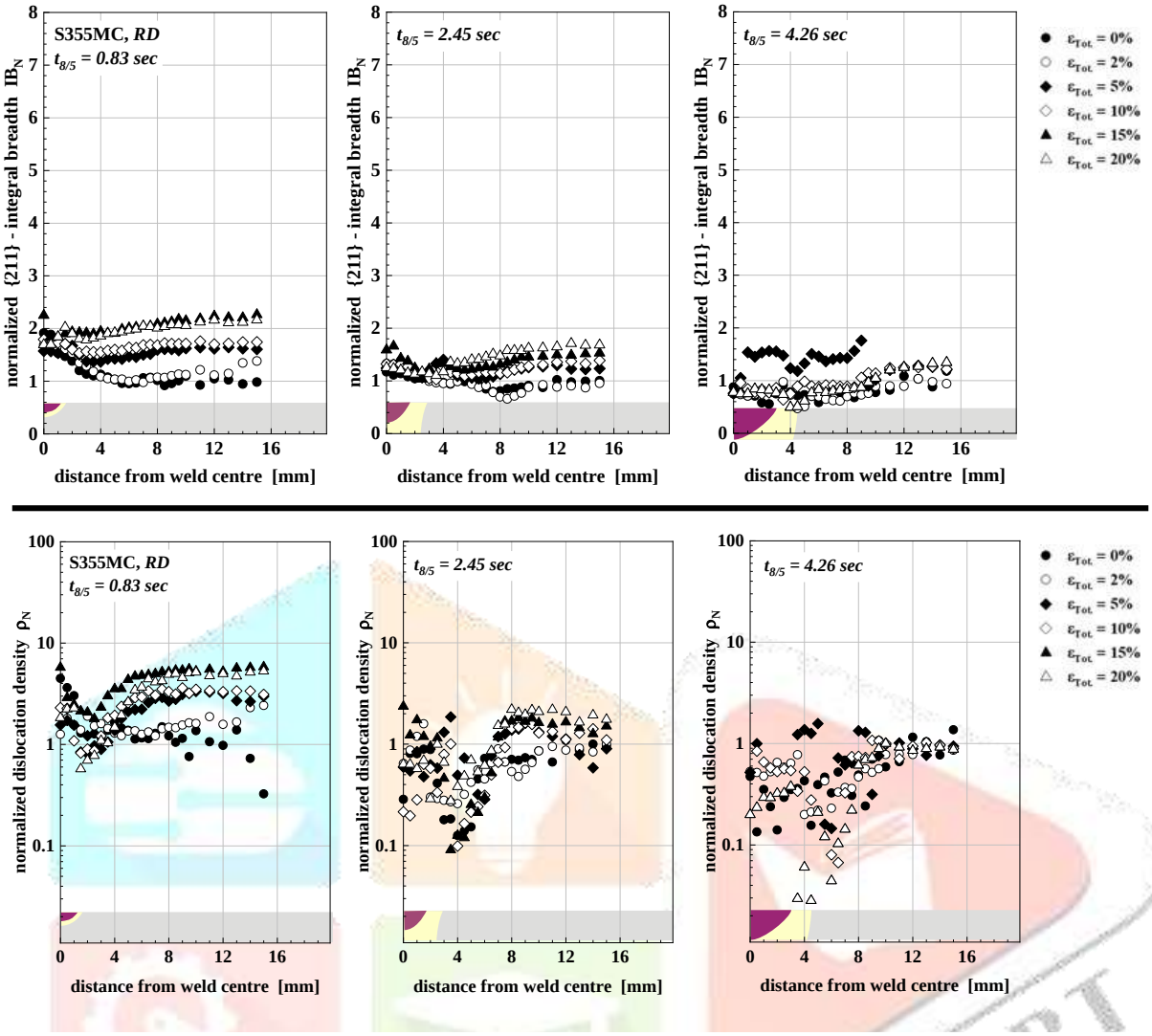

Fig. 13 Integral Breadth (Top) and Dislocation Density for the Martensite/Ferrite Phase (Bottom) of S355MC Under Varying Heat Input (Increased from Left to Right) for Different Deformation Grades (normalized to the non-deformed base material)

Comparing Strength Parameters Calculated from Different Methods:

The basic idea of this investigation was to work out, if the local strength condition and its changes due to the welding induced inhomogeneous thermal load can be described in an appropriate manner using non-destructively determinable parameters, namely with the characteristics of the measured X-ray diffraction lines. The general assumption was that the IB distributions (the value commonly used for this is the full width at half maximum (FWHM)) and those of the local hardness are similar, since in the present case the same microstructural mechanisms are responsible. This means that the distributions in the vicinity of the welds and materials investigated here show a uniform qualitative behavior. That means moreover that also the distributions parameters derived from the detailed X-ray diffraction line profile analysis, such as domain size, micro-strains, and calculated dislocation density, should also show similar courses. Then each of these parameters should be usable for the comprehensive qualitative description of the local strength condition compared to destructive hardness measurements. For this purpose, a dimensionless strength parameter V_H

$$V_H = \frac{Z - Z_{min}}{Z_{max} - Z_{min}}$$

is established, where H is a placeholder for each mentioned parameter (used indices: Vickers-hardness HV, integral breadth IB, indentation depth ´ind.´, dislocation density ρ, etc.), Z refers to the local measured values among total values for variable of a specific material, such as hardness, indentation depth, or integral

breadth. Z_{min} and Z_{max} represent the minimum and maximum values within the total measuring range, respectively. This equation scales the hardening within a range of 0 to 1. It should also be considered that the existence of inaccurately measured values, or so-called out-of-range data, can slightly shift the entire data set up or down in the diagram. However, this shift does not affect the overall distribution of the data set .

In Fig. 14 and Fig. 15, the parameters V_H on the basis of integral breadth, Vickers-hardness and indentation depth were used exemplarily for the HCT690T and the X40MnCrAlV 19 2.5 2 steel in order to compare their characteristics and therefore the applicability of such an approach. The diagrams illustrate the distribution of strengthening parameters along welded samples at varying elongation rates using different measuring methods.

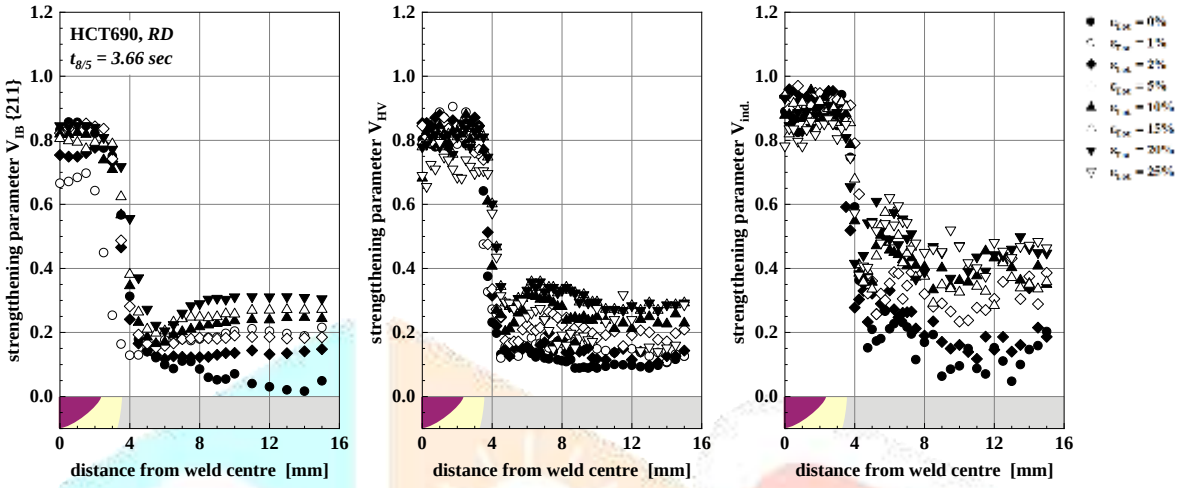

Fig. 14 Dimensionless Strengthening Parameters of HCT690T Calculated from (Left) Integral Breadth, (Middle) Hardness, and (Right) Indentation Test Method Under Constant Energy Input in Different Deformation Grades

The results demonstrate that the distribution trends are remarkably consistent across all measuring methods, confirming a linear correlation between each pair of data sets. It should be noted that the calculated indentation values were transposed along y-axis to facilitate accurate comparison with the other parameters. This adjustment ensures a coherent evaluation across the different methods used.

The strengthening characteristic of the X40MnCrAlV 19 2.5 2 steel under a medium range welding energy is shown in Fig. 15. Same as for the HCT690T steel, the observed results indicate consistent distribution trends across all measuring methods, highlighting a linear correlation between each pair of data sets. The comparison with HCT690T results shows that the strengthening factor for X40MnCrAlV 19 2.5 2 is significantly higher in the base material area. This strengthening potential of X40MnCrAlV 19 2.5 2 is corroborated by its more pronounced cold work strengthening, as illustrated in Fig. 2. Such enhanced mechanical performance suggests that X40MnCrAlV 19 2.5 2 is more effective in improving strength under these conditions. However, the observed softening in the welding area, indicative of a reduction in hardness, underscores the complex thermal responses of these materials.

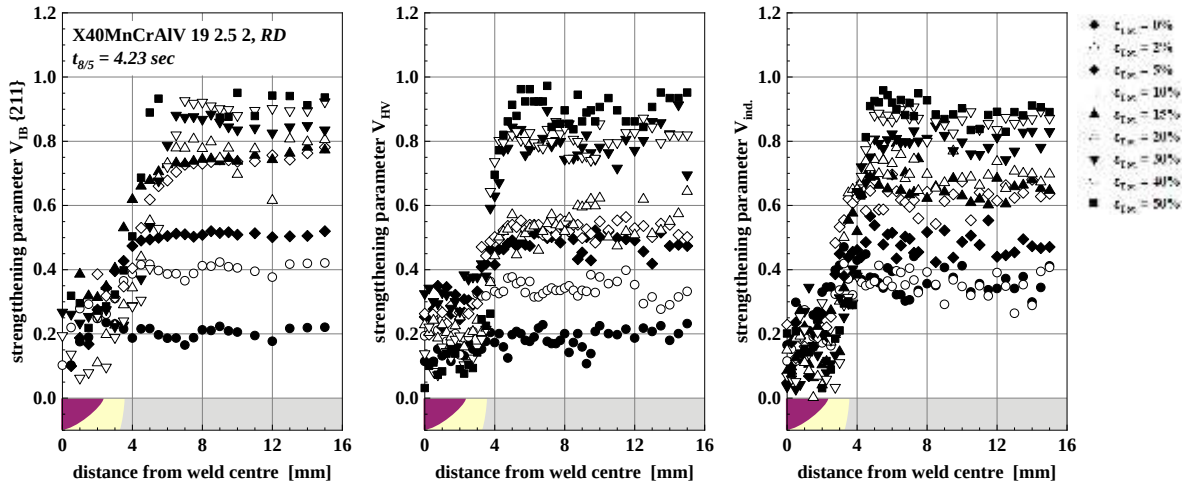

Fig. 15 Dimensionless Strengthening Parameters of X40MnCrAlV 19 2.5 2 Calculated from (Left) Integral Breadth, (Middle) Hardness, and (Right) Indentation Test Method Under Constant Energy Input in Different Deformation Grades

4 Conclusion

This study comprehensively examines the effects of welding on cold-formed steels, with a focus on the interaction between deformation-induced strengthening and thermal softening across three steel grades: HCT690T, X40MnCrAlV 19 2.5 2, and S355MC. Through hardness testing, instrumented microindentation testing, and X-ray diffraction line profile analysis, we observed distinct behaviors in these steels under deformation and welding conditions.

Notably, HCT690T exhibited substantial strengthening due to martensitic transformation induced by deformation, which remained stable post-welding. This robustness, confirmed by consistent peak broadening and increased dislocation density in X-ray diffraction analysis, underscores HCT690T's suitability for applications where high strength and thermal resistance are crucial.

In contrast, steel X40MnCrAl 19 2.5 2 shows softening in the weld seam post-deformation, likely due to the altered microstructure from melting and solidification during welding. The observed decrease in peak width at elevated temperatures suggests grain coarsening and lowered dislocation density. However, outside the weld seam, this steel demonstrated substantial hardening, indicating the need for optimized welding parameters to preserve its mechanical properties effectively.

S355MC, serving as a reference material, demonstrated minimal changes in the weld zone and slight increases in hardness in the base material, possibly due to minor microstructural changes or stress relaxation from welding heat.

Our findings emphasize the necessity of considering material-specific responses to thermal cycles and mechanical stresses in welding and structural design. Additionally, the introduction of a dimensionless strengthening parameter provides a standardized criterion for assessing strengthening states across different methods, enhancing evaluation precision. Overall, balancing deformation-induced strengthening and thermally induced softening is pivotal in optimizing welding practices and improving the performance of high-strength steels in industrial applications. Future research may explore refined welding techniques and advanced materials to further enhance the stability and performance of welded structures.

5 Acknowledgments

The results presented in this study were achieved as part of a collaborative effort between the Technical University of Braunschweig and the Karlsruhe Institute of Technology, supported by the German Research Foundation (DFG) under project numbers Gi376/17-1 and Ni508/19-1. The authors gratefully acknowledge the financial support provided by the German Research Foundation.

6 References

[1] Abbaschian R. Abbaschian L, Reed-Hill R, Physical Metallurgy Principles, 2009.

[2] N.J. den Uijl, L.J. Carless, Advanced metal-forming technologies for automotive applications, in: Advanced Materials in Automotive Engineering, Elsevier, 2012, pp. 28–56.

[3] B.C. de Cooman, High Mn TWIP steel and medium Mn steel, in: Automotive Steels, Elsevier, 2017, pp. 317–385.

[4] O. Grässel, G. Frommeyer, Effect of martensitic phase transformation and deformation twinning on mechanical properties of Fe–Mn–Si–AI steels, Materials Science and Technology 14 (1998) 1213–1217.

[5] L. Krüger, T. Halle, L.W. Meyer, U. Brüx, G. Frommeyer, Werkstoffverhalten und Mikrostrukturentwicklung hochfester Mn-Al-Si-Leichtbaustähle unter Zugbelastung, Mat.-wiss. u. Werkstofftech. 36 (2005) 299–306.

[6] M.F. Ashby, The deformation of plastically non-homogeneous materials, The Philosophical Magazine: A Journal of Theoretical Experimental and Applied Physics 21 (1970) 399–424.

[7] A. Pichler, S. Traint, H. Pauli, H. Mildner, J. Szinyur, M. Blaimschein, P. Stiaszny, and E.A. Werner, Processing and properties of cold rolled TRIP steels, 43rd Mechanical Working and Steel Processing Conference (2001) 411–434.

[8] G. Frommeyer, Entwicklung hochfester und supraduktiler Leichtbaustähle für die Verkehrstechnik, Max-Planck-Institut für Eisenforschung (2008).

[9] O. Grässel, L. Krüger, G. Frommeyer, L. Meyer, High strength Fe–Mn–(Al, Si) TRIP/TWIP steels development — properties — application, International Journal of Plasticity 16 (2000) 1391–1409.

[10] M. Kuntz, Verformungsmechanismen hoch manganlegierter austenitischer TWIP-Stähle, Dissertation, University of Stuttgart, 2007.

[11] I. Gutierrez-Urrutia, D. Raabe, Grain size effect on strain hardening in twinning-induced plasticity steels, Scripta Materialia 66 (2012) 992–996.

[12] S.W. Song, J.H. Lee, H.J. Lee, C.M. Bae, C.S. Lee, Enhancing high-cycle fatigue properties of cold-drawn Fe–Mn–C TWIP steels, International Journal of Fatigue 85 (2016) 57–64.

[13] D. Keil, Beitrag zur Schweißeignung hoch manganhaltiger Stähle, Dissertation, University Magdeburg, 2014.

[14] S. Kou, Welding metallurgy, 2nd ed., Wiley-Interscience, Hoboken N.J., 2003.

[15] O. Bouaziz, S. Allain, C.P. Scott, P. Cugy, D. Barbier, High manganese austenitic twinning induced plasticity steels: A review of the microstructure properties relationships, Current Opinion in Solid State and Materials Science 15 (2011) 141–168.

[16] V. Lazic, A. Sedmak, M. Zivkovic, S. Aleksandrovic, R. Cukic, R. Jovicic et al., Theoretical-experimental determining of cooling time (t8/5) in hard facing of steels for forging dies, Therm sci 14 (2010) 235–246.

[17] Takeshi Sawa, Correlation between Nanoindentation Test Result and Vickers Hardness (2010) 171–174.

[18] J. Gubicza, X-Ray Line Profile Analysis in Materials Science, IGI Global, 2014.

[19] V. Hauk (Ed.), Structural and Residual Stress Analysis by Nondestructive Methods, Elsevier Science B.V, Amsterdam, 1997.

[20] Paul S. Prevey, Lambda Research, X-Ray Diffraction Residual Stress Techniques, Metals Park: American Society for Metals (1986) 380–392.

[21] E04 Committee, Standard Test Method for X-Ray Determination of Retained Austenite in Steel with Near Random Crystallographic Orientation, ASTM International, West Conshohocken, PA. doi:10.1520/E0975-22.

[22] DIN EN ISO 6507-1, Metallische Werkstoffe –Härteprüfung nach Vickers –Teil 1: Prüfverfahren (ISO 6507-1:2023); Deutsche Fassung EN ISO 6507-1:2023.

[23] DIN EN ISO 14577-1, Metallische Werkstoffe –Instrumentierte Eindringprüfung zur Bestimmung der Härte und anderer Werkstoffparameter –Teil 1: Prüfverfahren (ISO/DIS 14577-1:2024); Deutsche und Englische Fassung prEN ISO 14577-1:2024.

[24] G. Guillonneau, J.M. Wheeler, J. Wehrs, L. Philippe, P. Baral, H.W. Höppel et al., Determination of the true projected contact area by in situ indentation testing, J. Mater. Res. 34 (2019) 2859–2868.

[25] A. Monsalve, F. de Barbieri, M. Gómez, A. Artigas, L. Carvajal, K. Sipos et al., Mechanical Behavior of a Twip Steel (Twinning Induced Plasticity), Matéria (Rio J.) 20 (2015) 653–658.

[26] S. Schmauder, C.-S. Chen, K.K. Chawla, N. Chawla, W. Chen, Y. Kagawa, Handbook of Mechanics of Materials, Springer Singapore, Singapore, 2019.

[27] Nico Hempel, Zum Einfluss zyklischer Plastizität auf die Eigenspannungsentstehung beim Schweißen hochlegierter Stähle, Dissertation, Technical University of Braunschweig (2022).